A Method for Simulating Two-Phase Pipe Flow with Real Equations of State

M. Hammer*, A. Morin

SINTEF Energy Research, P.O. Box 4761 Sluppen, NO-7465 Trondheim, Norway

Abstract

Common two-fluid models for pipe flow assume local non-equilibrium regarding phase transfer. To solve the two-fluid models together with accurate equations of state for real fluids will in most cases require mechanical, thermal and chemical equilibrium between the phases. The reason is that reference equations of state for real substances typically describe full thermodynamic equilibrium. In this paper, we present a method for numerically solving an equilibrium model analysed by Morin and Flåtten in the paper *A two-fluid four-equation model with instantaneous thermodynamical equilibrium*, 2013.

The four-equation two-fluid model with instantaneous thermodynamical equilibrium is derived from a five-equation two-fluid model with instantaneous thermal equilibrium. The four-equation model has one mass equation common for both phases, but allows for separate phasic velocities. For comparison, the five-equation two-fluid model is numerically solved, using source terms to impose thermodynamical equilibrium. These source terms are solved using a fractional-step method.

We employ the highly accurate Span-Wagner equation of state for CO_2, and use the simple and robust FORCE scheme with MUSCL slope limiting. We demonstrate that second-order accuracy may be achieved for smooth solutions, whereas the first-order version of the scheme even allows for a robust transition to single-phase flow, also in the presence of instantaneous phase equilibrium.

Keywords: two-fluid model, finite volume, FORCE scheme, Span-Wagner equation of state, isochoric–isoenergetic flash

1. Introduction

In the frame of CO_2 capture and storage (CCS), large amounts of CO_2 have to be transported between the point of capture and the point of injection. In the two-degree scenario of the International Energy Agency [1], about seven gigatonnes of CO_2 emissions will be contained using CCS in 2050. This requires the development of an extensive CO_2 transport network. For large volumes of CO_2, pipeline transport is an option.

There are challenges related to the operation of a CO_2 pipeline, both in normal operation and during depressurisation events, either planned or accidental. The safety of operation has to be ensured, and it has to be demonstrated to the regulatory bodies.

*Corresponding author. Tel.: +47 735 97 251

Email addresses: morten.hammer [a] sintef.no (M. Hammer), alexandre.morin [a] sintef.no (A. Morin)

To facilitate this, and to reduce costly experimental procedures, reliable and accurate numerical simulation tools have to be developed.

In pipelines, the CO_2 will generally be transported in a dense phase, supercritical or liquid. However, during transient events, gas or solid phases may appear. In addition, impurities from the capture process will be present in the CO_2. These impurities may be for example water, residual chemicals or gases from combustion. They will impact the thermodynamic behaviour of the CO_2, for example the mixture density or the temperature of the mixture during phase change.

It is common to use the stiffened-gas equations of state, when modelling two-phase flow [2, 3, 4, 5]. It has a simple analytical form, and can be used to describe metastable fluids. For long pipelines transporting CO_2 rich multi-component mixtures from a capture cite to an offshore injection well, these models might not predict the fluid properties accurately. In this case it is important to use real equations of state. The real equations of state are generally only valid for full thermodynamical equilibrium.

At least two types of transient events have to be studied, with very different characteristics. The first type covers the fast depressurisation events that occur when the pipe content is discharged to the atmosphere, either due to shutting down the pipeline, or due to a fracture [6]. The second type covers the load variations in the pipeline in normal operation, due to the capture processes delivering varying amounts of CO_2. These load variations will have time scales in the order of several hours.

The kinetics of heat transfer between the phases, and of phase change can most probably not be neglected in fast transients related to fast depressurisation events. However, during slow transients related to load variation, one is interested in predicting the response of the mixture in the pipeline, to avoid too low temperatures or phase change through pumps for example. During these slow transients, the most important is to have a very accurate equation of state to describe CO_2-rich mixtures, rather than to describe the kinetics of internal heat transfer or phase change very accurately. The time scales of these processes are negligible compared to the time scale of the relatively slow load variation. Very accurate equations of state can be obtained for mixtures at equilibrium. Thus it seems to be reasonable to use a full-equilibrium fluid-dynamical model in this case, to be able to benefit from the equilibrium equations of state.

Therefore, in the present work, we study full equilibrium fluid-dynamical models where phase change and heat transfer between the phases are assumed to be instantaneous. The framework supports any equation of state, thus impurities may be added by using an equation of state for mixtures. Here we are using a very accurate equation of state for pure CO_2 [7]. We compare two approaches. The first one is based on a fluid-dynamical model out of chemical equilibrium, the two-fluid five-equation model with phase change [8]. Instantaneous phase change is achieved by performing flash calculations between each time step, such that the mixture returns to chemical equilibrium. The second one is based on a full-equilibrium two-fluid four-equation model presented in [9].

Numerical results are presented to show the performance of the methods, and to compare them to each other. The models have been solved using the finite-volume method with the FORCE flux [10, Sec. 14.5.1] and the second-order extension MUSCL [11]. They show that the four-equation based approach performs better in terms of computational time than the five-equation based approach. It also shows that we can achieve second-order convergence rate in smooth regions, and that the method satisfactorily handles the transition to single-phase flow.

In Section 2, the five-equation model is presented, as well as the procedure to ensure chemical equilibrium between the phases. Then, the four-equation model is presented

in Section 3. In Section 4, the equation of state as well as the procedure to evaluate the new state of the fluid are explained. The characteristic wave-structure of the models are presented in Section 5. Subsequently, the numerical methods employed to solve the transport systems are described in Section 6. Finally, Section 7 shows the results of the numerical test cases, and Section 8 summarise this work.

2. The five-equation model with phase change

The one-dimensional two-fluid models describe one-dimensional two-phase flows in pipes. In the six-equation model, the phases are at mechanical equilibrium [8]. This means that the two phases are at the same pressure at all times. The model is well known in the literature [12, 13, 4, 14, 15], and used in commercial simulation tools like CATHARE [16] or RELAP5 [17].

The five-equation model [8] is derived from the six-equation model by assuming instantaneous thermal equilibrium. This means that the phases are now at the same pressure and temperature at all times. This model contains one mass and one momentum equation for each phase, while only one mixture energy equation is present. This model is similar to the model used by the commercial flow simulation tool OLGA [18]. When viscous terms are neglected, and all external forces but gravity are ignored, the system of equations for the one-dimensional five-equation model becomes

$$\frac{\partial(\rho_\mathrm{g}\alpha_\mathrm{g})}{\partial t} + \frac{\partial(\rho_\mathrm{g}\alpha_\mathrm{g}v_\mathrm{g})}{\partial x} = \Psi, \tag{1}$$

$$\frac{\partial(\rho_\ell\alpha_\ell)}{\partial t} + \frac{\partial(\rho_\ell\alpha_\ell v_\ell)}{\partial x} = -\Psi, \tag{2}$$

$$\frac{\partial(\rho_\mathrm{g}\alpha_\mathrm{g}v_\mathrm{g})}{\partial t} + \frac{\partial(\rho_\mathrm{g}\alpha_\mathrm{g}v_\mathrm{g}^2)}{\partial x} + \alpha_\mathrm{g}\frac{\partial p}{\partial x} + \tau_\mathrm{i} = v_\mathrm{i}\Psi + \rho_\mathrm{g}\alpha_\mathrm{g}g_x, \tag{3}$$

$$\frac{\partial(\rho_\ell\alpha_\ell v_\ell)}{\partial t} + \frac{\partial(\rho_\ell\alpha_\ell v_\ell^2)}{\partial x} + \alpha_\ell\frac{\partial p}{\partial x} - \tau_\mathrm{i} = -v_\mathrm{i}\Psi + \rho_\ell\alpha_\ell g_x, \tag{4}$$

$$\frac{\partial(E_\mathrm{g}+E_\ell)}{\partial t} + \frac{\partial(E_\mathrm{g}v_\mathrm{g}+\alpha_\mathrm{g}v_\mathrm{g}p)}{\partial x} + \frac{\partial(E_\ell v_\ell+\alpha_\ell v_\ell p)}{\partial x} = g_x\alpha_\mathrm{g}\rho_\mathrm{g}v_\mathrm{g} + g_x\alpha_\ell\rho_\ell v_\ell, \tag{5}$$

where the total energy E_k of phase $\mathrm{k} \in \{\mathrm{g}, \ell\}$ is the sum of kinetic and internal energy,

$$E_\mathrm{k} = \rho_\mathrm{k}\alpha_\mathrm{k}\left(\frac{1}{2}v_\mathrm{k}^2 + e_\mathrm{k}\right). \tag{6}$$

e is the specific internal energy.

Further, ρ is the mass density, v is the velocity, p is the pressure, α is the volume fraction, and g_x is the gravitational component along the x-axis. Ψ is the mass-transfer rate from the liquid to the gas phase, τ_i is the interfacial momentum exchange and v_i is the interfacial momentum velocity. The volume fractions must satisfy

$$\alpha_\mathrm{g} + \alpha_\ell = 1. \tag{7}$$

The interfacial momentum exchange is modelled with a differential term. In this term, the factor Δp represents the difference between the average bulk pressure and the pressure at the gas-liquid interface. In this work we use

$$\tau_\mathrm{i} = -\Delta p\frac{\partial\alpha_\ell}{\partial x}. \tag{8}$$

For practical simulations, Δp should be physically modelled to account, for example, for the hydrostatic pressure in the liquid phase, or for the interfacial tension. However, for the purpose of the general model analysis performed in the present article, Δp is here chosen to be [19, 8]

$$\Delta p = \delta \frac{\alpha_\mathrm{g}\alpha_\ell\rho_\mathrm{g}\rho_\ell}{\alpha_\ell\rho_\mathrm{g} + \alpha_\mathrm{g}\rho_\ell}(v_\mathrm{g} - v_\ell)^2, \tag{9}$$

where $\delta = 2$.

The unknowns of the system (1)–(5) are α_g, α_ℓ, v_g, v_ℓ, p, ρ_g, ρ_ℓ, e_g and e_ℓ. However, since we will be using the equation of state to solve the system, the temperature T must be included in the list. We have thus 10 unknowns. The 10 equations are (7), the transport equations (1)–(5), plus two thermodynamic relations per phase given by the equation of state.

We may split the system (1)–(5) into two parts, which will prove useful in the course of the article. The first part is the flow model (1)–(5) where phase change is ignored ($\Psi = 0$), while the second part only contains the contributions of phase change

$$\frac{\partial(\rho_\mathrm{g}\alpha_\mathrm{g})}{\partial t} = \Psi, \tag{10}$$

$$\frac{\partial(\rho_\ell\alpha_\ell)}{\partial t} = -\Psi, \tag{11}$$

$$\frac{\partial(\rho_\mathrm{g}\alpha_\mathrm{g}v_\mathrm{g})}{\partial t} = v_\mathrm{i}\Psi, \tag{12}$$

$$\frac{\partial(\rho_\ell\alpha_\ell v_\ell)}{\partial t} = -v_\mathrm{i}\Psi. \tag{13}$$

The energy equation has disappeared in the second system, because mixture energy is not concerned by phase change, it is only an internal transfer.

The speed of sound of this model is [8, 9]

$$c_{\mathrm{TF5}} = \sqrt{\frac{\alpha_\mathrm{g}\rho_\ell + \alpha_\ell\rho_\mathrm{g}}{\rho_\mathrm{g}\rho_\ell\left(\frac{\alpha_\mathrm{g}}{\rho_\mathrm{g}c_\mathrm{g}^2} + \frac{\alpha_\ell}{\rho_\ell c_\ell^2} + \frac{\alpha_\mathrm{g}\rho_\mathrm{g}C_{p,\mathrm{g}}\alpha_\ell\rho_\ell C_{p,\ell}T\left(\frac{\Gamma_\mathrm{g}}{\rho_\mathrm{g}c_\mathrm{g}^2} - \frac{\Gamma_\ell}{\rho_\ell c_\ell^2}\right)^2}{\alpha_\mathrm{g}\rho_\mathrm{g}C_{p,\mathrm{g}} + \alpha_\ell\rho_\ell C_{p,\ell}}\right)}}, \tag{14}$$

where c_k is the single-phase speed of sound of phase k, and $C_{p,\mathrm{k}}$ is its specific heat capacity and Γ_k its first Grüneisen parameter, defined by

$$\Gamma_\mathrm{k} = \frac{1}{\rho_\mathrm{k}}\frac{\partial p}{\partial e_\mathrm{k}}\bigg|_{\rho_\mathrm{k}} = \frac{1}{C_{V,\mathrm{k}}\rho_\mathrm{k}}\frac{\partial p}{\partial T}\bigg|_{\rho_\mathrm{k}}. \tag{15}$$

Remark that the speed of sound is only a function of the differential terms. It is not affected by the algebraic source terms modelling phase change.

2.1. Phase change

In the five-equation model (1)–(5) described above, the phases are generally out of chemical equilibrium. The mass transfer rate Ψ should then make the chemical potentials of the phases μ_k converge towards each other through phase change. A common way is to set the mass-transfer proportional to the difference in chemical potential [20, 21, 22],

$$\Psi = \mathcal{K}\left(\mu_\ell - \mu_\mathrm{g}\right), \quad \mathcal{K} \geq 0. \tag{16}$$

If the potential of the liquid phase μ_ℓ is greater than that of the gas phase μ_g, mass will be transferred from the liquid phase to the gas phase and vice versa, at a rate proportional to $\mathcal{K}$.

The phase change will also be accompanied by a transfer of momentum between the phases, while the mixture momentum will be conserved. Writing the part of the system (10)–(13) – which performs phase change – in differential form, we obtain

$$\mathrm{d}\left(\sum_\mathrm{k} (\rho\alpha v)_\mathrm{k}\right) = 0, \tag{17}$$

$$\mathrm{d}(\rho\alpha v)_\mathrm{g} = \mathrm{d}(\rho\alpha)_\mathrm{g}\, v_\mathrm{i}, \tag{18}$$

where

$$\mathrm{d}(\rho\alpha)_\mathrm{g} = \Psi\, \mathrm{d}t. \tag{19}$$

2.2. The interface velocity

Morin and Flåtten [9] showed that if the interfacial velocity v_i is independent of the chemical potentials, the expression

$$v_\mathrm{i} = \frac{1}{2}\left(v_\mathrm{g} + v_\ell\right), \tag{20}$$

is the only one which ensures that mass change will never decrease the entropy of the flow. Remark also that the following differential relations can be written

$$\mathrm{d}m_\mathrm{g} = -\,\mathrm{d}m_\ell, \tag{21}$$

$$\mathrm{d}(mv)_\mathrm{g} = \frac{1}{2}\left(v_\mathrm{g} + v_\ell\right)\mathrm{d}m_\mathrm{g}, \tag{22}$$

$$\mathrm{d}(mv)_\ell = \frac{1}{2}\left(v_\mathrm{g} + v_\ell\right)\mathrm{d}m_\ell, \tag{23}$$

$$\mathrm{d}(mv)_\mathrm{g} = \mathrm{d}(mv)_\ell \tag{24}$$

where $m_\mathrm{k} = (\rho\alpha)_\mathrm{k}$ is the phase mass per volume. Then, developing the total differential for the kinetic energy

$$\mathrm{d}\left(\frac{1}{2}\frac{(mv)_\mathrm{g}^2}{m_\mathrm{g}} + \frac{1}{2}\frac{(mv)_\ell^2}{m_\ell}\right) = v_\mathrm{g}\,\mathrm{d}(mv)_\mathrm{g} - \frac{1}{2}v_\mathrm{g}^2\,\mathrm{d}m_\mathrm{g} + v_\ell\,\mathrm{d}(mv)_\ell - \frac{1}{2}v_\ell^2\,\mathrm{d}m_\ell, \tag{25}$$

in which we substitute the relations (21), (22) and (23), we find that

$$\mathrm{d}\left(\frac{1}{2}m_\mathrm{g}v_\mathrm{g}^2 + \frac{1}{2}m_\ell v_\ell^2\right) = 0. \tag{26}$$

Thus, as noted by Stewart and Wendroff in [23], the kinetic energy of the mixture is not affected by phase change. This means that the model (1)–(5) can first be solved without phase change (system (1)–(5) with $\Psi = 0$), before the phase fractions are updated through phase change in a separate step. If the kinetic energy had been affected by the mass transfer, we would have had to solve simultaneously the thermodynamic equilibrium and the phasic velocities.

2.3. Instantaneous phase change

If phase change may be assumed to be instantaneous ($\mathcal{K} \to \infty$ in (16)), an equilibrium equation of state (EOS) may be used. Such an EOS describes multiphase mixtures at equilibrium. For example, the Span-Wagner EOS [7] is very accurate for CO_2 in gas, liquid and supercritical phases. One possible approach is to take advantage of the remark above. After the model (1)–(5) without phase change ($\Psi = 0$) has evolved for one time step, the two phases will in general be out of chemical equilibrium. The second part of the time step is therefore to come back to equilibrium through phase change (system (10)–(13)). This approach is a fractional-step method [24, p. 380], also called a time-splitting strategy [25, 4].

First, the phasic masses have to be determined so that the mixture is at equilibrium. The mixture mass is given as the sum of phasic masses, (1) and (2), and the overall energy is given from (5). Using the result from (26), the internal energy can be calculated. The resulting problem is to solve a constant density and internal energy (isochoric–isoenergetic) flash. Since there is a momentum transfer between the phases, the new phasic velocities then have to be determined. We can write the equations expressing the conservation of the mixture momentum and mixture kinetic energy as

$$(mv)_{\mathrm{g}}^{\mathrm{n}^*} + (mv)_{\ell}^{\mathrm{n}^*} = (mv)_{\mathrm{g}}^{n} + (mv)_{\ell}^{n}\,, \tag{27}$$

$$\frac{1}{2}\left(mv^2\right)_{\mathrm{g}}^{\mathrm{n}^*} + \frac{1}{2}\left(mv^2\right)_{\ell}^{\mathrm{n}^*} = \frac{1}{2}\left(mv^2\right)_{\mathrm{g}}^{n} + \frac{1}{2}\left(mv^2\right)_{\ell}^{n}\,, \tag{28}$$

where n^* represents the state before applying phase change, and n is the state after applying phase change.

This gives a quadratic equation for the velocities. Its discriminant Δ is written as

$$\Delta = m_{\ell}^{n} m_{\mathrm{g}}^{n} m_{\ell}^{\mathrm{n}^*} m_{\mathrm{g}}^{\mathrm{n}^*} \left(v_{\mathrm{g}}^{\mathrm{n}^*} - v_{\ell}^{\mathrm{n}^*}\right)^2, \tag{29}$$

which is never negative, so that we will always have real roots. The roots of v_{ℓ}^{n} are

$$v_{\ell}^{n} = v_{\mathrm{m}}^{n} \pm \frac{\left|v_{\mathrm{g}}^{\mathrm{n}^*} - v_{\ell}^{\mathrm{n}^*}\right| \sqrt{m_{\ell}^{n} m_{\mathrm{g}}^{n} m_{\ell}^{\mathrm{n}^*} m_{\mathrm{g}}^{\mathrm{n}^*}}}{m_{\ell}^{n}\left(m_{\mathrm{g}}^{\mathrm{n}^*} + m_{\ell}^{\mathrm{n}^*}\right)} \tag{30}$$

where

$$v_{\mathrm{m}}^{n} = \frac{m_{\mathrm{g}}^{\mathrm{n}^*} v_{\mathrm{g}}^{\mathrm{n}^*} + m_{\ell}^{\mathrm{n}^*} v_{\ell}^{\mathrm{n}^*}}{m_{\mathrm{g}}^{\mathrm{n}^*} + m_{\ell}^{\mathrm{n}^*}} \tag{31}$$

may be defined as the mixture velocity. A criterion is now required to select the correct root. Equations (21) and (23) give

$$dv_{\ell} = \frac{dm_{\mathrm{g}}}{2m_{\ell}}\left(v_{\ell} - v_{\mathrm{g}}\right), \tag{32}$$

while the differentiation of (30) with respect to m_{g}^{n} evaluated for $m_{\ell}^{n} = m_{\ell}^{\mathrm{n}^*}$ provides the relation

$$dv_{\ell}^{n} = \pm \frac{dm_{\mathrm{g}}^{n}}{2m_{\ell}^{\mathrm{n}^*}} \left|v_{\mathrm{g}}^{\mathrm{n}^*} - v_{\ell}^{\mathrm{n}^*}\right|. \tag{33}$$

Comparing equations (32) and (33), the correct root for v_{ℓ}^{n} can be determined, and is

$$v_{\ell}^{n} = v_{\mathrm{m}}^{n} + \frac{\left(v_{\ell}^{\mathrm{n}^*} - v_{\mathrm{g}}^{\mathrm{n}^*}\right) \sqrt{m_{\ell}^{n} m_{\mathrm{g}}^{n} m_{\ell}^{\mathrm{n}^*} m_{\mathrm{g}}^{\mathrm{n}^*}}}{m_{\ell}^{n}\left(m_{\mathrm{g}}^{\mathrm{n}^*} + m_{\ell}^{\mathrm{n}^*}\right)}. \tag{34}$$

Now, the gas velocity can be expressed as a function of the liquid velocity, and the gas velocity, v_{g}^{n}, becomes

$$v_{\mathrm{g}}^{n} = v_{\mathrm{m}}^{n} - \frac{\left(v_{\ell}^{\mathrm{n}^*} - v_{\mathrm{g}}^{\mathrm{n}^*}\right)\sqrt{m_{\ell}^{n} m_{\mathrm{g}}^{n} m_{\ell}^{\mathrm{n}^*} m_{\mathrm{g}}^{\mathrm{n}^*}}}{m_{\mathrm{g}}^{n}\left(m_{\mathrm{g}}^{\mathrm{n}^*} + m_{\ell}^{\mathrm{n}^*}\right)}. \tag{35}$$

Remark that in the case of a single-phase flow, we have $v_{\ell}^{n} = v_{\mathrm{m}}^{n}$ and $v_{\mathrm{g}}^{n} = v_{\mathrm{m}}^{n}$.

Note that the mass-transfer rate Ψ is never explicitly evaluated. The flash calculation implicitly transfers mass from one phase to the other so that the mixture is at equilibrium.

2.4. Integration procedure

To summarise, the integration of the system (1)–(5) from time step $n-1$ to time step n is split in four steps, introducing an intermediate time step, n^*.

1. Integrate the system (1)–(5) where phase change is ignored ($\Psi = 0$) from time step $n-1$ to n^*. The composite variables, $(\alpha\rho v)_{\ell}^{\mathrm{n}^*}$, $(\alpha\rho v)_{\mathrm{g}}^{\mathrm{n}^*}$, $(\alpha\rho)_{\ell}^{\mathrm{n}^*}$, $(\alpha\rho)_{\mathrm{g}}^{\mathrm{n}^*}$, and $E^{\mathrm{n}^*} = (E_{\mathrm{g}} + E_{\ell})^{\mathrm{n}^*}$ are then known.
2. Calculate mixture density,
$$\rho_{\mathrm{m}}^{n} = \sum_{\mathrm{k}\in\{\mathrm{g},\ell\}} (\rho\alpha)_{\mathrm{k}}^{\mathrm{n}^*}, \tag{36}$$
and mixture internal energy,
$$(\rho e)_{\mathrm{m}}^{n} = E^{\mathrm{n}^*} - \frac{1}{2}\sum_{\mathrm{k}\in\{\mathrm{g},\ell\}} \frac{\left[(\rho\alpha v)_{\mathrm{k}}^{\mathrm{n}^*}\right]^2}{(\rho\alpha)_{\mathrm{k}}^{\mathrm{n}^*}}, \tag{37}$$
using composite variables from the intermediate time step n^*. Further, calculate $T^{n}, \alpha_{\mathrm{g}}^{n}\alpha_{\ell}^{n}, \rho_{\mathrm{g}}^{n}$ and ρ_{ℓ}^{n} by solving a isochoric–isoenergetic flash given the mixture density and internal energy. This problem will be further described in Section 4. The pressure is then given by the thermodynamics, $p^{n} = p(T^{n}, \rho_{\mathrm{g}}^{n}) = p(T^{n}, \rho_{\ell}^{n})$.
3. Calculate new velocities v_{g}^{n} and v_{ℓ}^{n} from equations (34) and (35).
4. Update the composite variables for momentum and mass ($(\alpha\rho v)_{\ell}^{n}$, $(\alpha\rho v)_{\mathrm{g}}^{n}$, $(\alpha\rho)_{\ell}^{n}$ and $(\alpha\rho)_{\mathrm{g}}^{n}$).

2.5. Vector expression of the model

To summarise, with some rearrangement of the derivatives, and introducing the enthalpy, $h = e + p/\rho$, we can write the five-equation model in vector form as

$$\frac{\partial \boldsymbol{u}}{\partial t} + \frac{\partial \boldsymbol{f}(\boldsymbol{u})}{\partial x} + \boldsymbol{B}(\boldsymbol{u})\frac{\partial \boldsymbol{w}(\boldsymbol{u})}{\partial x} = \boldsymbol{s}(\boldsymbol{u}), \tag{38}$$

where

$$\boldsymbol{u} = \begin{bmatrix} \alpha_\mathrm{g}\rho_\mathrm{g} \\ \alpha_\ell\rho_\ell \\ \alpha_\mathrm{g}\rho_\mathrm{g}v_\mathrm{g} \\ \alpha_\ell\rho_\ell v_\ell \\ E_\mathrm{g} + E_\ell \end{bmatrix}, \quad \boldsymbol{f}(\boldsymbol{u}) = \begin{bmatrix} \alpha_\mathrm{g}\rho_\mathrm{g}v_\mathrm{g} \\ \alpha_\ell\rho_\ell v_\ell \\ \alpha_\mathrm{g}\rho_\mathrm{g}v_\mathrm{g}^2 + \alpha_\mathrm{g}\Delta p \\ \alpha_\ell\rho_\ell v_\ell^2 + \alpha_\ell\Delta p \\ \sum_\mathrm{k}\alpha_\mathrm{k}\rho_\mathrm{k}v_\mathrm{k}\left(\frac{1}{2}v_\mathrm{k}^2 + h_\mathrm{k}\right) \end{bmatrix},$$

$$\boldsymbol{s}(\boldsymbol{u}) = \begin{bmatrix} \Psi \\ -\Psi \\ \frac{1}{2}\left(v_\mathrm{g} + v_\ell\right)\Psi + \rho_\mathrm{g}\alpha_\mathrm{g}g_x \\ -\frac{1}{2}\left(v_\mathrm{g} + v_\ell\right)\Psi + \rho_\ell\alpha_\ell g_x \\ g_x\sum_\mathrm{k}\alpha_\mathrm{k}\rho_\mathrm{k}v_\mathrm{k} \end{bmatrix}, \quad \boldsymbol{B}(\boldsymbol{u}) = \begin{bmatrix} 0 \\ 0 \\ \alpha_\mathrm{g} \\ \alpha_\ell \\ 0 \end{bmatrix}, \tag{39}$$

$$\boldsymbol{w}(\boldsymbol{u}) = \begin{bmatrix} p - \Delta p \end{bmatrix}.$$

2.6. Algebraic source terms and wave propagation

In the fractional-step method described in Section 2.4 the flux part of the model, $\boldsymbol{f}(\boldsymbol{u})$ and $\boldsymbol{w}(\boldsymbol{u})$ in (39), is solved alternately with the algebraic part $\boldsymbol{s}(\boldsymbol{u})$. Now, the algebraic source terms should affect the propagation of the waves predicted by the flux part of the model. This does not happen explicitly in the present method. The waves predicted by the flux-based solver are corrected *a posteriori* using the source terms. Particularly, instantaneous phase change slows down the intrinsic mixture speed of sound of the model. Thus, the speed of sound (14) over-estimates the actual speed of sound of the model with instantaneous phase change. Now, the speed of sound is used in the stability criterion of the scheme – the CFL number – thus the time steps are unnecessarily short. By including instantaneous phase change in the flux part of the system, we obtain a more faithful mixture speed of sound, thus the numerical methods can use larger time steps. This reduces the simulation time.

3. The four-equation model

We now want to derive a four-equation model which is equivalent to the five-equation model (1)–(5) when the phase change is instantaneous. The transformation described in the following is used to integrate the algebraic source terms in the fluxes, giving a full-equilibrium model.

3.1. Expression of the system

The full-equilibrium fluid-dynamical model is obtained by summing the two mass equations (3) and (4), and adding the constraint that the phasic chemical potentials should be equal to each other at all times. This leads to the two-fluid four-equation

model with instantaneous phase change [9]

$$\frac{\partial(\rho_{\mathrm{g}}\alpha_{\mathrm{g}}+\rho_{\ell}\alpha_{\ell})}{\partial t}+\frac{\partial(\rho_{\mathrm{g}}\alpha_{\mathrm{g}}v_{\mathrm{g}}+\rho_{\ell}\alpha_{\ell}v_{\ell})}{\partial x}=0, \tag{40}$$

$$\frac{\partial(\rho_{\mathrm{g}}\alpha_{\mathrm{g}}v_{\mathrm{g}})}{\partial t}+\frac{\partial(\rho_{\mathrm{g}}\alpha_{\mathrm{g}}v_{\mathrm{g}}^2)}{\partial x}+\alpha_{\mathrm{g}}\frac{\partial p}{\partial x}+\tau_{\mathrm{i}}+v_{\mathrm{i}}\mathcal{K}\left(\mu_{\mathrm{g}}-\mu_{\ell}\right)=\rho_{\mathrm{g}}\alpha_{\mathrm{g}}g_x, \tag{41}$$

$$\frac{\partial(\rho_{\ell}\alpha_{\ell}v_{\ell})}{\partial t}+\frac{\partial(\rho_{\ell}\alpha_{\ell}v_{\ell}^2)}{\partial x}+\alpha_{\ell}\frac{\partial p}{\partial x}-\tau_{\mathrm{i}}-v_{\mathrm{i}}\mathcal{K}\left(\mu_{\mathrm{g}}-\mu_{\ell}\right)=\rho_{\ell}\alpha_{\ell}g_x, \tag{42}$$

$$\frac{\partial(E_{\mathrm{g}}+E_{\ell})}{\partial t}+\frac{\partial(E_{\mathrm{g}}v_{\mathrm{g}}+\alpha_{\mathrm{g}}v_{\mathrm{g}}p)}{\partial x}+\frac{\partial(E_{\ell}v_{\ell}+\alpha_{\ell}v_{\ell}p)}{\partial x}=g_x\alpha_{\mathrm{g}}\rho_{\mathrm{g}}v_{\mathrm{g}}+g_x\alpha_{\ell}\rho_{\ell}v_{\ell}. \tag{43}$$

Now, since the phase change is instantaneous and $\mu_{\mathrm{g}}=\mu_{\ell}$, the term $\mathcal{K}\left(\mu_{\mathrm{g}}-\mu_{\ell}\right)$ is undefined. The analysis in [9] shows that it takes the form

$$\mathcal{K}\left(\mu_{\mathrm{g}}-\mu_{\ell}\right)=\mathcal{V}(\boldsymbol{u})\frac{\partial\left(\alpha_{\mathrm{g}}v_{\mathrm{g}}+\alpha_{\ell}v_{\ell}\right)}{\partial x}+\mathcal{P}(\boldsymbol{u})\frac{\partial p}{\partial x} \tag{44}$$

in the limit $\mathcal{K}\to\infty$, where it is assumed that

$$v_{\mathrm{i}}=\frac{\left(v_{\mathrm{g}}+v_{\ell}\right)}{2}. \tag{45}$$

The expressions $\mathcal{V}(\boldsymbol{u})$ and $\mathcal{P}(\boldsymbol{u})$ are given by

$$\mathcal{V}(\boldsymbol{u})=\frac{\rho_{\mathrm{g}}\rho_{\ell}}{\alpha_{\ell}\rho_{\mathrm{g}}+\alpha_{\mathrm{g}}\rho_{\ell}}\frac{T}{L}\left(\alpha_{\mathrm{g}}\rho_{\mathrm{g}}C_{p,\mathrm{g}}\chi_{\mathrm{g}}+\alpha_{\ell}\rho_{\ell}C_{p,\ell}\chi_{\ell}\right)c_{\mathrm{TF4}}^2, \tag{46}$$

and

$$\mathcal{P}(\boldsymbol{u})=\frac{\alpha_{\mathrm{g}}\alpha_{\ell}\rho_{\mathrm{g}}\rho_{\ell}(v_{\mathrm{g}}-v_{\ell})}{\alpha_{\ell}\rho_{\mathrm{g}}+\alpha_{\mathrm{g}}\rho_{\ell}}\frac{T}{L}\left(\rho_{\ell}C_{p,\ell}\chi_{\ell}\frac{\psi_{\mathrm{g}}}{\rho_{\mathrm{g}}c_{\mathrm{g}}^2}-\rho_{\mathrm{g}}C_{p,\mathrm{g}}\chi_{\mathrm{g}}\frac{\psi_{\ell}}{\rho_{\ell}c_{\ell}^2}\right)c_{\mathrm{TF4}}^2, \tag{47}$$

where the speed of sound of the four-equation two-fluid model is

$$c_{\mathrm{TF4}}=\sqrt{\frac{\alpha_{\ell}\rho_{\mathrm{g}}+\alpha_{\mathrm{g}}\rho_{\ell}}{\rho_{\mathrm{g}}\rho_{\ell}\left(\frac{\alpha_{\mathrm{g}}}{\rho_{\mathrm{g}}c_{\mathrm{g}}^2}+\frac{\alpha_{\ell}}{\rho_{\ell}c_{\ell}^2}+T\left(\alpha_{\mathrm{g}}\rho_{\mathrm{g}}C_{p,\mathrm{g}}\chi_{\mathrm{g}}^2+\alpha_{\ell}\rho_{\ell}C_{p,\ell}\chi_{\ell}^2\right)\right)}}, \tag{48}$$

and the following shorthands have been used

$$\chi_{\mathrm{g}}=\frac{\Gamma_{\mathrm{g}}}{\rho_{\mathrm{g}}c_{\mathrm{g}}^2}+\frac{\rho_{\mathrm{g}}-\rho_{\ell}}{\rho_{\mathrm{g}}\rho_{\ell}L}, \tag{49}$$

$$\chi_{\ell}=\frac{\Gamma_{\ell}}{\rho_{\ell}c_{\ell}^2}+\frac{\rho_{\mathrm{g}}-\rho_{\ell}}{\rho_{\mathrm{g}}\rho_{\ell}L}, \tag{50}$$

$$\psi_{\mathrm{k}}=1+\rho_{\mathrm{k}}TC_{p,\mathrm{k}}\Gamma_{\mathrm{k}}\chi_{\mathrm{k}}, \tag{51}$$

$$L=h_{\mathrm{g}}-h_{\ell}. \tag{52}$$

The momentum exchange between the phases τ_{i} remains the same as in the five-equation model, and is modelled as in (8).

3.2. Vector form of the model

To summarise, the four-equation model can be written in vector form

$$\frac{\partial \boldsymbol{u}}{\partial t} + \frac{\partial \boldsymbol{f}(\boldsymbol{u})}{\partial x} + \boldsymbol{B}(\boldsymbol{u}) \frac{\partial \boldsymbol{w}(\boldsymbol{u})}{\partial x} = \boldsymbol{s}(\boldsymbol{u}), \tag{53}$$

where

$$\begin{aligned}
\boldsymbol{u} &= \begin{bmatrix} \alpha_\mathrm{g}\rho_\mathrm{g} + \alpha_\ell\rho_\ell \\ \alpha_\mathrm{g}\rho_\mathrm{g}v_\mathrm{g} \\ \alpha_\ell\rho_\ell v_\ell \\ E_\mathrm{g} + E_\ell \end{bmatrix}, \quad \boldsymbol{f}(\boldsymbol{u}) = \begin{bmatrix} \alpha_\mathrm{g}\rho_\mathrm{g}v_\mathrm{g} + \alpha_\ell\rho_\ell v_\ell \\ \alpha_\mathrm{g}\rho_\mathrm{g}v_\mathrm{g}^2 + \alpha_\mathrm{g}\Delta p \\ \alpha_\ell\rho_\ell v_\ell^2 + \alpha_\ell\Delta p \\ \sum_\mathrm{k}\alpha_\mathrm{k}\rho_\mathrm{k}v_\mathrm{k}\left(\frac{1}{2}v_\mathrm{k}^2 + h_\mathrm{k}\right) \end{bmatrix}, \\
\boldsymbol{s}(\boldsymbol{u}) &= \begin{bmatrix} 0 \\ \rho_\mathrm{g}\alpha_\mathrm{g}g_x \\ \rho_\ell\alpha_\ell g_x \\ g_x\sum_\mathrm{k}\alpha_\mathrm{k}\rho_\mathrm{k}v_\mathrm{k} \end{bmatrix}, \quad \boldsymbol{B}(\boldsymbol{u}) = \begin{bmatrix} 0 & 0 & 0 \\ v_\mathrm{i}\mathcal{V} & \alpha_\mathrm{g} + v_\mathrm{i}\mathcal{P} & -\alpha_\mathrm{g} \\ -v_\mathrm{i}\mathcal{V} & \alpha_\ell - v_\mathrm{i}\mathcal{P} & -\alpha_\ell \\ 0 & 0 & 0 \end{bmatrix}, \\
\boldsymbol{w}(\boldsymbol{u}) &= \begin{bmatrix} \alpha_\mathrm{g}v_\mathrm{g} + \alpha_\ell v_\ell \\ p \\ \Delta p \end{bmatrix}.
\end{aligned} \tag{54}$$

4. Algorithm to evaluate the primitive variables

When the model have been advanced one time step, only the new composite variable vector $\boldsymbol{u}$ is known. However, to evaluate the fluxes ($\boldsymbol{f}(\boldsymbol{u})$, $\boldsymbol{w}(\boldsymbol{u})$) and the coefficients of $\boldsymbol{B}(\boldsymbol{u})$ in (39) and (54), the primitive variables (pressure, temperature, gas volume fraction, phasic velocities, phasic internal energies) have to be known. In the present section, we will first present the EOS used to evaluate the thermodynamical state of the mixture. Then we will explain how the primitive variables are calculated.

4.1. The Span-Wagner reference equation of state for CO_2

The Span-Wagner reference EOS comprises an expression for the CO_2 Helmholtz free energy $a(T, \rho)$ [7]. The reduced non-dimensional Helmholtz free energy equation

$$\Phi(\tau, \delta) = \frac{a(\tau, \delta)}{RT} = \Phi^0(\tau, \delta) + \Phi^\mathrm{r}(\tau, \delta), \tag{55}$$

is composed of an ideal contribution, Φ^0, and a residual contribution, Φ^r. R is the universal gas constant. The reduced Helmholtz functions are expressed in terms of the reduced density, $\delta = \rho/\rho_\mathrm{crit}$, and inverse reduced temperature, $\tau = T_\mathrm{crit}/T$, where ρ_crit and T_crit are the critical density and the critical temperature, respectively. The expression for the reduced ideal part is

$$\begin{aligned}
\Phi^0(\tau, \delta) = \ln(\delta) + a_1^0 + a_2^0\tau + a_3^0\ln(\tau) \\
+ \sum_{i=4}^{8} a_i^0 \ln\left[1 - \exp\left(-\tau\theta_i^0\right)\right].
\end{aligned} \tag{56}$$

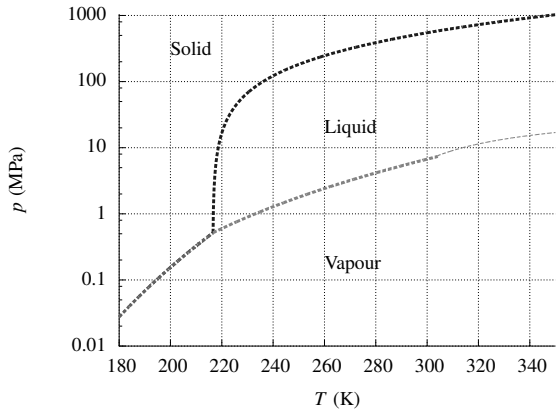

Figure 1: Phase diagram for CO_2.

The expression for the reduced residual part is

$$\begin{aligned}\Phi^{\mathrm{r}}(\tau,\delta) = &\sum_{i=1}^{7} n_i \delta^{d_i} \tau^{t_i} \\ &+ \sum_{i=8}^{34} n_i \delta^{d_i} \tau^{t_i} \exp\left(-\delta^{c_i}\right) \\ &+ \sum_{i=35}^{39} n_i \delta^{d_i} \tau^{t_i} \exp\left(-\alpha_i (\delta-\varepsilon_i)^2 - \beta_i (\tau-\gamma_i)^2\right) \\ &+ \sum_{i=40}^{42} n_i \Delta^{b_i} \delta \exp\left(-C_i (\delta-1)^2 - D_i (\tau-1)^2\right),\end{aligned} \tag{57}$$

where $\Delta = \{(1-\tau)+A_i[(\delta-1)^2]^{1/(2B_i)}\}^2 + B_i[(\delta-1)^2]^{a_i}$. In this work the same coefficients $a_i^0, \theta_i^0, n_i, a_i, b_i, c_i, d_i, t_i, \alpha_i, \beta_i, \varepsilon_i, \gamma_i, A_i, B_i, C_i$ and D_i as published in [7], are used.

By differentiation of the Helmholtz function, all required thermodynamic properties can be derived. The differentials for the CO_2 Helmholtz function are found in the original paper by Span and Wagner [7]. As seen from equations (56)–(57), the Span-Wagner EOS contains many terms, including logarithms and exponentials, making it computationally demanding.

The Span-Wagner EOS is valid from the triple-point temperature to 1100 K and for pressures up to 800 MPa. Span and Wagner also provided auxiliary equations for the sublimation line and the fusion line. These equations are used together with the saturation line calculated from the Helmholtz function for pure CO_2 to plot the phase diagram in Figure 1. The dotted line continuing the saturation line above the critical pressure and temperature represents $(\partial^2 P/\partial\rho^2)_T = 0$. The triple and critical point of CO_2 are displayed in Table 1. Pressures/temperatures for the test cases are selected at the saturation line in the range between the triple and critical point.

4.2. Five-equation model

To calculate the primitive variables for the five-equation model, the procedure from Section 2.4 is applied. The most challenging and CPU intensive part of the procedure

Table 1: Critical and triple point of CO_2. Data taken from [7].

Property	Symbol	Value
Critical temperature	T_{crit}	304.1282 K
Critical pressure	P_{crit}	7.3773 MPa
Triple point temperature	T_{tr}	216.592 K
Triple point pressure	P_{tr}	0.51795 MPa

is step 2, where intensive properties, T and P as well as the phase fractions must be calculated. Thermodynamically, the equilibrium condition of this isochoric–isoenergetic (ρe) problem represents a global maximum in the entropy of the system [26]. The numerical algorithm used to solve the ρe problem are based on the method of Giljarhus et al. [27], and discussed in more detail in Hammer et al. [28].

In this work only single-phase, liquid or gas, and liquid-gas equilibrium are considered. The single-phase equation is simply

$$e(T, \rho_{\text{spec}}) - e_{\text{spec}} = 0, \tag{58}$$

where ρ_{spec} and e_{spec} are the specified density and specific internal energy. Equation (58) must be solved for the unknown temperature, T. It should be noted that solving Equation 58 can produce a meta-stable solution. In case of a meta-stable solution, there exists a liquid-gas solution with higher entropy. The single-phase solution must therefore be tested for stability. If introduction of a new phase give an increase in entropy, the single phase solution is discarded, and a liquid-gas solution is sought instead.

To solve the ρe problem for liquid in equilibrium with gas, both the equilibrium conditions, $P_{\text{g}} = P_\ell$ and $\mu_{\text{g}} = \mu_\ell$, and the density and internal energy specification equations must be fulfilled:

$$P(T, \rho_{\text{g}}) - P(T, \rho_\ell) = 0, \tag{59}$$

$$\mu(T, \rho_{\text{g}}) - \mu(T, \rho_\ell) = 0, \tag{60}$$

$$z_{\text{g}} e(T, \rho_{\text{g}}) + (1 - z_{\text{g}}) e(T, \rho_\ell) - e_{\text{spec}} = 0, \tag{61}$$

$$\frac{z_{\text{g}}}{\rho_{\text{g}}} + \frac{(1 - z_{\text{g}})}{\rho_\ell} - \frac{1}{\rho_{\text{spec}}} = 0. \tag{62}$$

Here z_{g} denotes the gas mass fraction. The unknowns of the liquid–gas equation system (59)–(62) are $[\rho_{\text{g}}, \rho_\ell, T, z_{\text{g}}]$.

Both (58) and the equation system (59)–(62) are solved using a second-order Newton method.

4.3. Four-equation model

The challenge for the four-equation model is that the distribution of the overall energy in kinetic and internal energy is not known *a priori*. It has to be evaluated through iterations. The proposed procedure to evaluate the primitive variables uses a successive substitution approach. Using j as iteration index, the procedure is as follows:

1. Assume, $m_{\text{g}}^{n+1,j=0} = m_{\text{g}}^n$ and $m_\ell^{n+1,j=0} = m_\ell^n$, and calculate the phasic velocities, $v_{\text{g}}^{n+1,j=0}$ and $v_\ell^{n+1,j=0}$, from the composite momentum variables.

2. Calculate $T^{n+1,j}$, $p^{n+1,j}$, $\alpha_{\mathrm{g}}^{n+1,j}$ and $\rho_{\mathrm{g}}^{n+1,j}$ etc. using composite variables for mass and energy. The same problem as described in Section 4.2 must be solved.
3. Calculate new velocities, $v_{\mathrm{g}}^{n+1,j+1}$ and $v_{\ell}^{n+1,j+1}$, from the new phase masses, $m_{\mathrm{g}}^{n+1,j+1}$ and $m_{\ell}^{n+1,j+1}$.
4. If $\left|m_{\mathrm{g}}^{n+1,j+1} - m_{\mathrm{g}}^{n+1,j}\right| < \epsilon$ exit loop. Otherwise increment j and repeat from step 2. $\epsilon = 10^{-11}$ have been used in all simulations.

5. Characteristic wave-structure of the models

The characteristic wave structure of the two-fluid models is not known in general. In the case of equal phasic velocities, two of the eigenvalues correspond to acoustic waves, while the remaining ones are equal to the mixture velocity. These waves are entropy and volume-fraction waves (cf. [29] for the six-equation model, [8] for the five-equation model and [9] for the four-equation model).

When relaxation source terms are added, the characteristic wave structure is no longer clearly defined [30]. However, when the relaxation becomes instantaneous, the characteristic wave structure converges to that of the relaxed system. Thus, by performing the instantaneous chemical relaxation of the five-equation model numerically, we expect to recover the structure of the four-equation model.

6. Numerical methods

The fluid-dynamical models are solved using the finite-volume method with the FORCE flux [10, Sec. 14.5.1]. The integration formula is

$$\frac{\boldsymbol{u}_i^{n+1} - \boldsymbol{u}_i^n}{\Delta t} + \frac{\boldsymbol{f}_{i+1/2}^{\mathrm{FO},n} - \boldsymbol{f}_{i-1/2}^{\mathrm{FO},n}}{\Delta x} = \boldsymbol{0}, \tag{63}$$

where $\boldsymbol{u}_i^n$ is the variable vector at time step n and in cell i. $\boldsymbol{f}_{i+1/2}^{\mathrm{FO},n}$ is the FORCE flux at time step n and at the interface $i + 1/2$. Δt and Δx are the time and spatial steps.

The FORCE flux [10, Sec. 14.5.1] combines two components. The first one is the very robust Lax-Friedrichs flux

$$\boldsymbol{f}_{i-1/2}^{\mathrm{LF}} = \frac{1}{2}\left(\boldsymbol{f}\left(\boldsymbol{u}_{i-1}\right) + \boldsymbol{f}\left(\boldsymbol{u}_i\right) - a\left(\boldsymbol{u}_i - \boldsymbol{u}_{i-1}\right)\right), \tag{64}$$

where the cell flux $\boldsymbol{f}(\boldsymbol{u})$ is given in Sections 2.5 and 3.2. $a = \Delta x/\Delta t$, and $a\left(\boldsymbol{u}_i - \boldsymbol{u}_{i-1}\right)$ plays the role of extra numerical viscosity. The second component in the FORCE flux is the Richtmyer flux. It is second-order accurate in smooth regions, however it produces oscillations at discontinuities. It is defined in two steps [10, Sec. 14.5.1]. First, an intermediate state is predicted as

$$\boldsymbol{u}_{i-1/2}^{\mathrm{Ri}} = \frac{1}{2}\left(\boldsymbol{u}_{i-1} + \boldsymbol{u}_i\right) - \frac{1}{2}\frac{\Delta t}{\Delta x}\left(\boldsymbol{f}\left(\boldsymbol{u}_i\right) - \boldsymbol{f}\left(\boldsymbol{u}_{i-1}\right)\right), \tag{65}$$

before the inter-cell flux is evaluated as

$$\boldsymbol{f}_{i-1/2}^{\mathrm{Ri}} = \boldsymbol{f}\left(\boldsymbol{u}_{i-1/2}^{\mathrm{Ri}}\right). \tag{66}$$

The FORCE flux is then defined as

$$\boldsymbol{f}_{i-1/2}^{\mathrm{FO}} = \frac{1}{2}\left(\boldsymbol{f}_{i-1/2}^{\mathrm{LF}} + \boldsymbol{f}_{i-1/2}^{\mathrm{Ri}}\right). \tag{67}$$

6.1. Second order with MUSCL

In a finite volume scheme, the solution is piecewise constant, making the method first order. By introducing a piecewise linear reconstruction of the solution, the method may be made second-order in smooth regions. Note that the scheme must go down to first order at extremas and discontinuities, to avoid oscillations. One approach is the monotone upwind-centred scheme for conservation laws (MUSCL) [11, 31]. We use a semidiscrete version, where a piecewise linear function, $\boldsymbol{l}$, is constructed at each side of the interface $x_{i-1/2}$,

$$\boldsymbol{u}_{i-1}^{\mathrm{R}} = \boldsymbol{u}_{i-1} + \frac{\Delta x}{2}\boldsymbol{l}_{i-1} \quad \text{and} \quad \boldsymbol{u}_{i}^{\mathrm{L}} = \boldsymbol{u}_{i} - \frac{\Delta x}{2}\boldsymbol{l}_{i}. \tag{68}$$

MUSCL is dependent on choosing the variables with which the solution is reconstructed. Here we chose $[\alpha_{\mathrm{g}}, P, v_{\mathrm{g}}, v_{\ell}]$. In the case of the five-equation model, the temperature is recovered as the saturation temperature at the given pressure. This is not possible when the flow is in a single phase state. Thus, here the second order extension is not used for flows that change from two-phase to single-phase.

To obtain a second-order solution in time, we employ the two-stage second-order strong-stability-preserving (SSP) Runge–Kutta (RK) method (see for instance [32]).

6.2. Non-conservative terms

The coefficient matrix of the non-conservative terms $\boldsymbol{B}_{j+1/2}$ has to be averaged at the interface between two cells. Finite-volume methods for systems of non-conservative transport equations are in general not yet able to converge to the right weak solution. In particular, the solution may fail to fulfil the Rankine-Hugoniot shock relations for shocks of very large amplitude [33, 34, 35]. However, Munkejord et al. [13] studied the effect of the averaging of $\boldsymbol{B}_{j+1/2}$ when solving the six-equation two-fluid model, and found that it was moderate. It is not in the scope of the present paper to discuss technical details regarding non-conservative terms. For simplicity, we choose to use the arithmetic average of a variable vector $\boldsymbol{q}$. Thus we have

$$\boldsymbol{B}_{j+1/2} = \boldsymbol{B}\left(\boldsymbol{u}\left(\boldsymbol{q}_{j+1/2}\right)\right), \tag{69}$$

where

$$\boldsymbol{q}_{j+1/2} = \frac{1}{2}\left(\boldsymbol{q}_{j} + \boldsymbol{q}_{j+1}\right). \tag{70}$$

There are several possible choices for $\boldsymbol{q}$. In the present work, we chose the same vector for both the five-equation and the four-equation models,

$$\boldsymbol{q} = \begin{bmatrix} \alpha_{\mathrm{g}} & v_{\mathrm{g}} & v_{\ell} & P \end{bmatrix}^{T}. \tag{71}$$

For the five-equation model, only α_{k} is used in the matrix $\boldsymbol{B}_{j+1/2}$, thus no special care has to be taken for the thermodynamic state. For the four-equation model, the mixture is at all time maintained at full equilibrium. Thus, the remaining variables in the matrix $\boldsymbol{B}_{j+1/2}$, like the saturation temperature T and the phase densities ρ_{ℓ} and ρ_{g}, can be calculated from the pressure P using the equation of state.

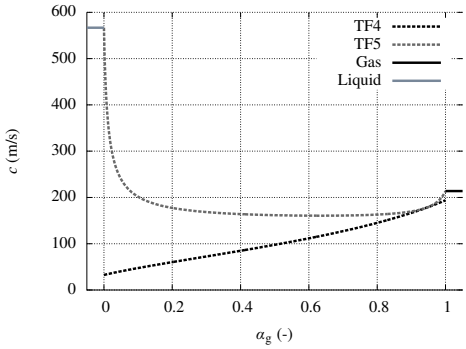

Figure 2: Speed of sound, c, plotted against gas volume fraction, α_g, at $T = 270\,\mathrm{K}$ and $P = 3.2033\,\mathrm{MPa}$ (saturation pressure at $T = 270\,\mathrm{K}$).

7. Numerical results

In the current section, we present numerical results for the four-equation and five-equation two-fluid models. A shock tube case is used to study the resolution of the wave propagation. A moving Gauss curve test case is presented to show the convergence order in smooth regions. It is also used to assess the performance of the two approaches in terms of computational time. A volume-fraction discontinuity propagating at constant velocity in a constant pressure field is used to test if the numerical scheme produces pressure and velocity oscillations at the discontinuity. A separation case shows how the four-equation model handles the transition to single-phase flow. Further, a two-phase expansion tube is used to simulate cavitation and expansion waves in the presence of equilibrium mass transfer. The volume-fraction discontinuity and the separation case are only simulated using the four-equation model.

For equation (9) the value $\delta = 2$ has been used in all simulations.

7.1. Speed of sound estimates

Figure 2 shows the speed of sound for the five-equation and four-equation models, plotted against the gas volume fraction at $T = 270\,\mathrm{K}$ and $P = 3.2033\,\mathrm{MPa}$. The speed of sound assuming phase equilibrium, c_{TF4} (48), is generally lower than the non-equilibrium speed of sound c_{TF5} (14). Note also that the speed of sound assuming full equilibrium is discontinuous at the transition to single phase. For example, the speed of sound in the liquid is close to $600\,\mathrm{m/s}$, but with the first bubble appearing, it drops to under $50\,\mathrm{m/s}$. This behaviour has already been noted in [20].

7.2. Shock tube

A shock tube is a case in which two constant states are separated by a single discontinuity. This is called a Riemann problem. When it evolves, a number of waves propagate from the initial discontinuity. The waves and their velocities are intrinsic properties of a system of transport equations, and numerical methods should be able to capture them. Concretely, the situation described by this test case is two half-tubes separated by a membrane, filled with fluid at rest, in different states, as illustrated in Figure 3. At $t = 0\,\mathrm{s}$, the membrane ruptures, the fluids are set in contact, and the flow starts evolving.

The case presented here consists of a horizontal $100\,\mathrm{m}$ tube. The initial conditions are given in Table 2. The initial temperatures are the saturation temperatures calculated

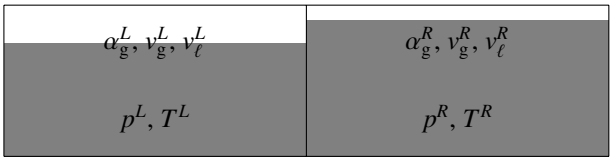

Figure 3: Shock tube.

Table 2: Initial state for CO_2 shock tube.

Quantity	Symbol (unit)	Left	Right
Gas vol. frac.	$\alpha_g\,(-)$	0.25	0.1
Pressure	$p\,(\mathrm{MPa})$	4.0	3.0
Gas velocity	$v_g\,(\mathrm{m/s})$	0	0
Liquid velocity	$v_\ell\,(\mathrm{m/s})$	0	0

from the initial pressures given in Table 2. The CFL number is 0.5. Figure 4 shows the results after the waves have evolved, with the four-equation model, and Figure 5 shows the results for the five-equation model. It can be seen that the curves are very similar, though not totally identical. They both converge to a solution with four visible waves. This is natural for the four-equation model. For the five-equation model, this is caused by the source terms that force the instantaneous equilibrium. They make one of the waves disappear, while the other waves converge to that of the four-equation model (cf. Section 5). The inaccuracies visible between the two middle waves on the velocity plots can be related to the inaccuracies visible in the shock-tube plots of [29]. They are believed to be caused by the non-conservative terms.

7.3. Moving Gauss curve

This test case has been designed to test the convergence order of the schemes for smooth solutions. It consists of a bubble of gas following the liquid in a horizontal pipe. Both phases initially have the same velocity and pressure. The gas volume fraction follows a Gauss curve profile

$$\alpha_{g,0} = (1 - 2\epsilon)\exp\left(-\frac{(x-\overline{x})^2}{2\sigma^2}\right) + \epsilon, \tag{72}$$

where $\sigma = 0.42\,\mathrm{m}$, $\overline{x} = 6\,\mathrm{m}$, and $\epsilon = 1 \times 10^{-7}$. When no source terms are present, a numerical scheme should preserve the uniform flow, that is, variations should not be introduced in the velocities or in the pressure. This has sometimes been referred to as the principle of Abgrall [36]. Thus, the gas volume-fraction profile should be advected without being altered.

The initial conditions are summarised in Table 3. The pressure is the saturation pressure corresponding to the initial temperature. Calculations have been performed with periodic boundary conditions until $t = 0.03\,\mathrm{s}$. The exact solution is then the same curve centred at $x = 9\,\mathrm{m}$. Figure 6 shows the gas volume-fraction profile after evolution with the four-equation model. We can see that the peak is eroded by numerical viscosity for the low grid resolutions. By comparing the profiles after evolution on different grid resolutions to the exact reference solution, we can evaluate the order of convergence.

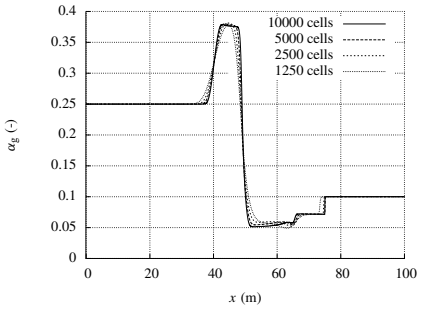

(a) Gas volume fraction.

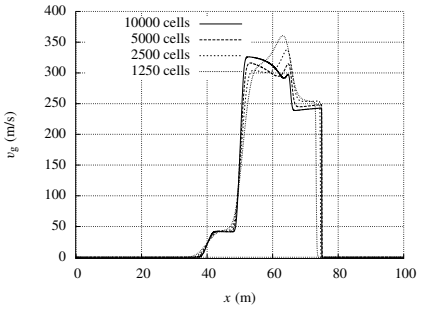

(b) Gas velocity.

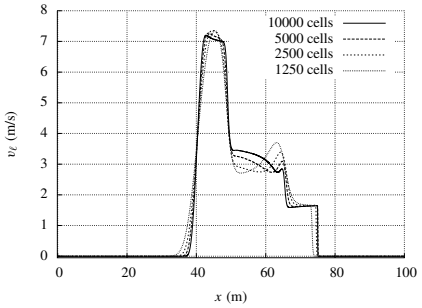

(c) Liquid velocity.

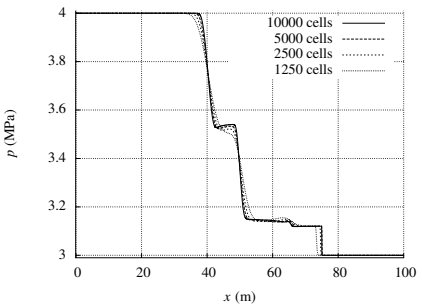

(d) Pressure.

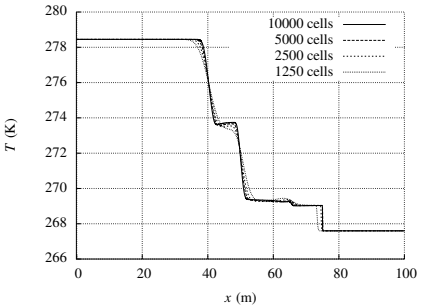

(e) Temperature.

Figure 4: CO_2 shock tube solved using the four-equation model. Result at $t = 0.15$ s using the CFL number 0.5. The Riemann problem is solved using the FORCE flux.

Table 3: Initial state for the moving Gauss curve.

Quantity	Symbol (unit)	Value
Gas vol. frac.	$\alpha_g\,(-)$	$\alpha_{g,0}(x)$
Pressure	p (MPa)	3.2033 (sat. pres.)
Temperature	T (K)	270
Gas velocity	v_g (m/s)	100
Liquid velocity	v_ℓ (m/s)	100

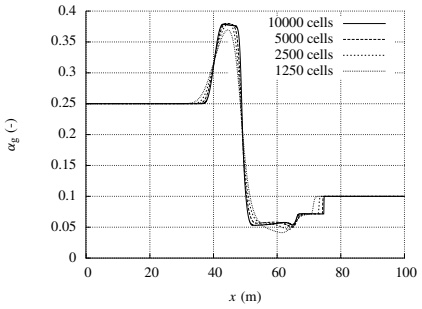

(a) Gas volume fraction.

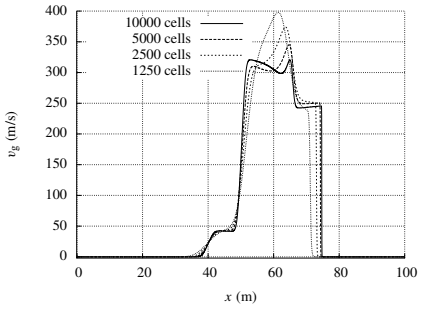

(b) Gas velocity.

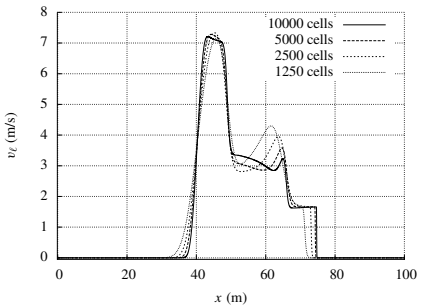

(c) Liquid velocity.

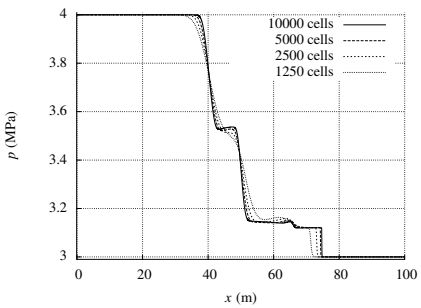

(d) Pressure.

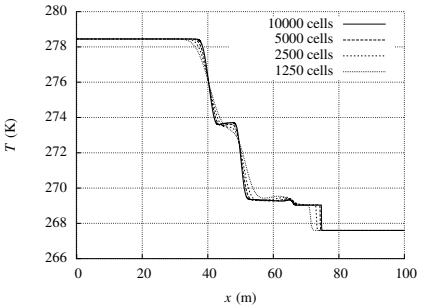

(e) Temperature.

Figure 5: CO_2 shock tube solved using the five-equation model. Result at $t = 0.15$ s using the CFL number 0.5. The Riemann problem is solved using the FORCE flux.

Table 4: Moving Gauss curve simulated using MUSCL-FORCE and second order RK time integration. Convergence order, $s_{\mathcal{N}}$, and 1–norm of the error in the gas volume fraction by grid refinement.

	TF4 MUSCL-FORCE		TF5 MUSCL-FORCE	
$\mathcal{N}(-)$	$\|\mathcal{E}(\alpha_g)\|_1$	$s_{\mathcal{N}}$	$\|\mathcal{E}(\alpha_g)\|_1$	$s_{\mathcal{N}}$
125	1.1412×10^{-1}	–	2.0145×10^{-1}	–
250	2.9719×10^{-2}	1.94	5.2551×10^{-2}	1.94
500	8.0421×10^{-3}	1.89	1.2690×10^{-2}	2.05
1000	2.0530×10^{-3}	1.97	3.0749×10^{-3}	2.05
2000	4.9704×10^{-4}	2.05	7.2381×10^{-4}	2.09
4000	1.1913×10^{-4}	2.06	1.6809×10^{-4}	2.10
8000	2.8316×10^{-5}	2.07	3.8658×10^{-5}	2.12

Table 5: Moving Gauss curve simulated using the FORCE flux and forward Euler in time. Convergence order, $s_{\mathcal{N}}$, and 1–norm of the error in the gas volume fraction by grid refinement.

	TF4 FORCE		TF5 FORCE	
$\mathcal{N}(-)$	$\|\mathcal{E}(\alpha_g)\|_1$	$s_{\mathcal{N}}$	$\|\mathcal{E}(\alpha_g)\|_1$	$s_{\mathcal{N}}$
125	7.2185×10^{-1}	–	1.1211	–
250	5.1865×10^{-1}	0.477	8.8405×10^{-1}	0.343
500	3.4618×10^{-1}	0.583	6.4475×10^{-1}	0.455
1000	2.1362×10^{-1}	0.696	4.2957×10^{-1}	0.586
2000	1.2288×10^{-1}	0.798	2.6186×10^{-1}	0.714
4000	6.6949×10^{-2}	0.876	1.4822×10^{-1}	0.821
8000	3.5146×10^{-2}	0.930	7.9587×10^{-2}	0.897

The error in the calculated gas volume fraction at a given time step has been quantified using the 1-norm

$$\|\mathcal{E}(\alpha_g)\|_1 = \Delta x \sum_{\forall j} |\alpha_{g,j} - \alpha_{g,\mathrm{ref},j}|, \tag{73}$$

where j is the cell index and the subscript "ref" indicates the exact reference solution. Then, the convergence order $s_{\mathcal{N}}$ for a number of cells $\mathcal{N}$ is estimated by

$$s_{\mathcal{N}} = \frac{\ln\left(\frac{\|\mathcal{E}(\alpha_g)\|_{1,\mathcal{N}}}{\|\mathcal{E}(\alpha_g)\|_{1,\mathcal{N}/2}}\right)}{\ln 2}. \tag{74}$$

Table 4 shows the results for the four-equation and five-equation models. As expected for the MUSCL-FORCE scheme, the convergence order is close to 2, since the solution is smooth. Here, the van Leer [11], limiter has been used.

Table 5 shows the results for the four-equation and five-equation models with the FORCE scheme. The convergence order is approaching 1.

The relevant comparison to evaluate the efficiency of a method is to compare the error in the solution to the CPU time used to arrive at the solution. The advantage of the five-equation-based approach is that the flashing problem is independent of the fluid-dynamical problem, thus simplifying the solution procedure. In the four-equation-based approach, the flashing problem and the kinetic energy problem must be

Table 6: Initial state for the moving volume-fraction discontinuity case. $\epsilon = 1 \times 10^{-7}$ is used.

Quantity	Symbol (unit)	Left	Right
Gas vol. frac.	α_g (−)	ϵ	$1 - \epsilon$
Pressure	p (MPa)	1.0	1.0
Temperature	p (K)	233.03 (sat. temp.)	233.03 (sat. temp.)
Gas velocity	v_g (m/s)	100	100
Liquid velocity	v_ℓ (m/s)	100	100

solved simultaneously, which requires an iterative solver. On the other hand, the four-equation-based approach is less prone to numerical diffusion, as the comparison of the absolute errors in Table 5 and 4 shows. Besides, the speed of sound in the four-equation model is lower than in the five-equation model, thus for the same CFL number, the time steps in the four-equation-based approach are larger. Figure 7 presents the comparison of the efficiencies. It shows that four-equation-based approach performs better. This is despite the fact that the primitive variables in the four-equation-based approach are solved using successive substitution. It is probable that a Newton algorithm would perform better, thus improving the global performance of the approach.

7.4. Moving volume-fraction discontinuity

A difficulty encountered by conservative finite-volume schemes for flow models with real equation of state is the occurence of pressure oscillations at interfaces. To demonstrate the capabilities of the four-equation-based approach, a numerical simulation of the moving discontinuity case proposed by Abgrall [36], and later used by Saurel et al. [37], is included. Like in the moving Gauss curve, the flow propagates at a constant velocity in a constant pressure field. In this case, a single volume-fraction discontinuity is propagated with the flow, instead of a volume fraction Gauss curve.

The initial conditions are summarised in Table 6. The volume-fraction discontinuity is simulated using 500 cells in a 1 m tube. The discontinuity is introduced at 0.5 m. The MUSCL–FORCE numerical flux is used, and zero order extrapolation of the tube state is applied for the ghost boundary cells. The van Leer [11] limiter has been used. After a simulation time of $t = 0.00279$ s, the resulting volume fraction, phasic velocities, mixture density and pressure are plotted in Figure 8. No pressure or velocity oscillations is seen at the volume-fraction discontinuity. Comparing the cell pressures, p_i, to the initial pressure, p^0, for all time steps n, the maximum relative error is

$$\frac{\max_{i,n} |p_i^n - p^0|}{p^0} < 10^{-11}. \tag{75}$$

7.5. Separation case

The separation case consists in letting the phases evolve in a vertical tube under the action of the gravity. The liquid phase will fall to the bottom, while the gas phase will be pushed to the top. This is illustrated in Figure 9. This is generally challenging for the numerical methods, due to the transition to single phase. The test case is presented to demonstrate the ability of the model to predict volume fractions exactly equal to 0 or 1. At that time, the single phase leaves the liquid-vapour equilibrium line.

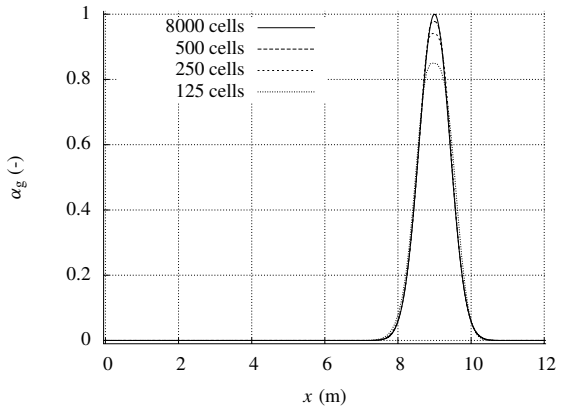

Figure 6: Moving Gauss curve. Four-equation model. Grid refinement for MUSCL–FORCE using the van Leer slope. CFL number 0.5. Results are plotted for $t = 0.03$ s.

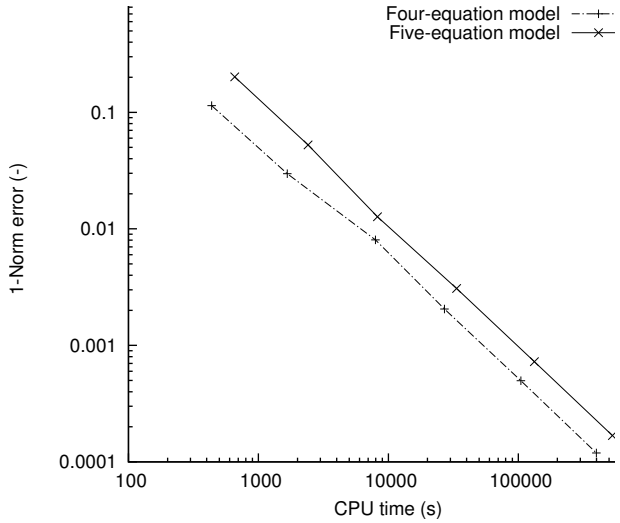

Figure 7: Error at $t = 0.03$ s for moving Gauss curve plotted against consumed CPU time. All simulations are performed using MUSCL–FORCE.

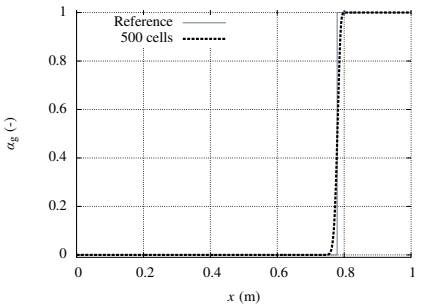

(a) Gas volume fraction.

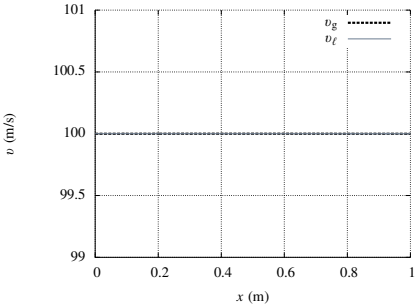

(b) Gas and liquid velocity.

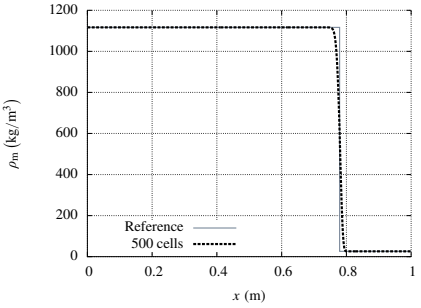

(c) Mixture density.

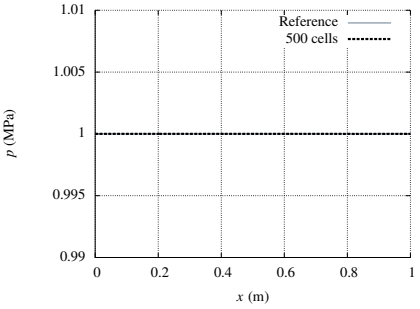

(d) Pressure.

Figure 8: Moving volume-fraction discontinuity using the four-equation model. Result at $t = 0.00279\,\mathrm{s}$ using CFL number 0.5 and 500 cells are plotted together with the reference solution. Reference solutions for the velocities, $v_g = v_\ell = 100\,\mathrm{m/s}$, are omitted. The Riemann problem is solved using MUSCL–FORCE flux.

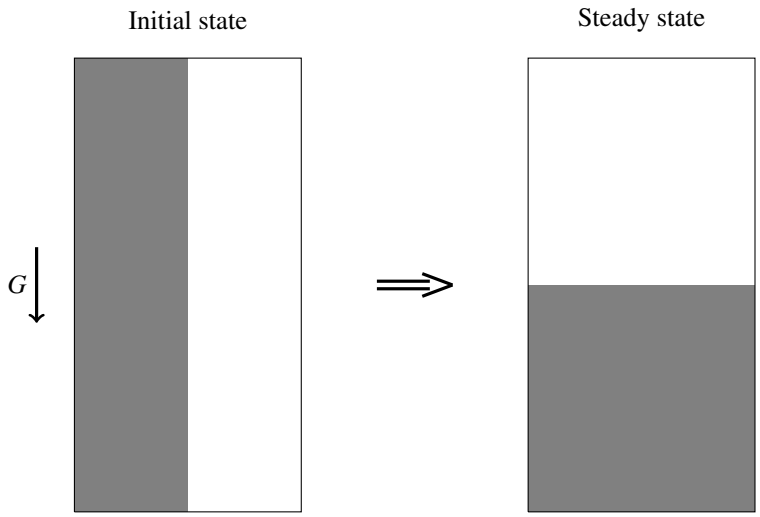

Figure 9: Separation case.

Table 7: Initial state for the separation case.

Quantity	Symbol (unit)	Value
Gas vol. frac.	α_g (−)	0.5
Pressure	p (MPa)	1
Temperature	T (K)	233.0274 (sat. temp.)
Gas velocity	v_g (m/s)	0
Liquid velocity	v_ℓ (m/s)	0

The initial conditions are summarised in Table 7. The gravity acceleration is taken to be $G = 3 \times 9.81\ \mathrm{m/s^2}$. The temperature is calculated as the saturation temperature at the initial pressure.

Results from a simulation of the separation case are shown in Figure 10. We can see that the gas volume fraction quickly goes to 0 at the bottom of the pipe (at the right-hand side of the Figure), while it goes to 1 at the top. There is a transition zone with two phases in between, which reduces with time.

In Figure 11, the pressure profile is plotted against the temperature profile at $t = 1\,\mathrm{s}$. The saturation line is also plotted. In the two-phase area, the mixture is on the saturation line. After the transition to one phase, the model manages to produce states outside of the saturation line. This is possible because the gas volume fraction reaches exactly 0 or 1. As long as $0 < \alpha_g < 1$, the mixture will always remain on the saturation line.

7.6. Two-phase expansion tube

Saurel et al. [22] simulated a two-phase expansion tube with water at 0.1 MPa, and relaxed the gas-liquid equilibrium in temperature and chemical potential. Here we consider a similar two-phase expansion tube case with gas and liquid CO_2 in equilibrium at 0.6 MPa.

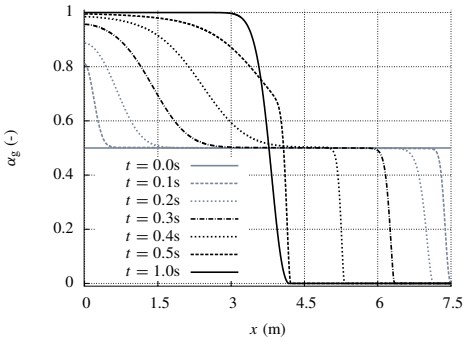

Figure 10: Separation case. The four equation model and the FORCE scheme is applied with CFL number 0.5, and 4000 cells. The gas volume fraction, α_{g}, profile is plotted at 7 different times.

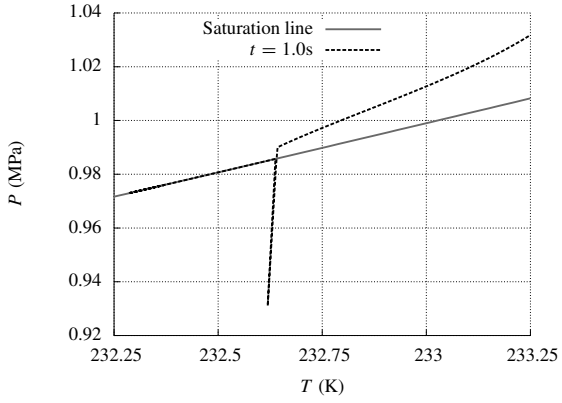

Figure 11: Separation case pressure plotted versus temperature at $t = 1.0$ s. The saturation pressure is also plotted, to illustrate where the the transition to single phase. The case is simulated using FORCE, CFL number 0.5, and 4000 cells.

Table 8: Initial state for the two-phase CO_2 expansion tube.

Quantity	Symbol (unit)	Left	Right
Gas vol. frac.	α_g (−)	0.01	0.01
Pressure	p (MPa)	0.6	0.6
Temperature	p (K)	220.0	220.0
Gas velocity	v_g (m/s)	−2.0	2.0
Liquid velocity	v_ℓ (m/s)	−2.0	2.0
Gas density	ρ_g (kg/m^3)	15.839	15.839
Liquid density	ρ_ℓ (kg/m^3)	1154.6	1154.6

Initially a 1 m long tube contains 1 % gas, $\alpha_g = 0.01$, uniformly distributed. Located at $x = 0.5$ m there is a velocity discontinuity. On the left side the velocity is set to $u_g = u_\ell = -2.0$ m/s, and on the right side the velocity is set to $u_g = u_\ell = 2.0$ m/s. The inital conditions are summarised in Table 8.

The MUSCL–FORCE numerical flux is used, and zero order extrapolation of the tube state is applied for the ghost boundary cells. The van Leer [11] limiter has been used. After a simulation time of $t = 0.03$ s, the resulting gas volume fraction, phasic velocites, mixture density and pressure are plotted in Figure 12. A CFL number of 0.5 was used.

Figure 12 shows one rarefaction wave traveling to the left and one to the right. These leading expansion waves are followed by two slower evaporation fronts. At $x = 0.5$ m a cavitation pocket forms, where the gas volume fraction become close to 1. The gas volume fraction increase due to gas expansion, phase transfer and partly by inflow of gas. Even if the two-phase expansion tube is simulated with CO_2 at full equilibrium, and at different conditions than by Saurel et al. [22], the same waves and the same qualitative behaviour is seen. From Figure 12a and 12b, it is seen that the five-equation model gives larger numerical diffusion than the four-equation model.

8. Summary

In the present work, we have numerically compared approaches to solve two different two-fluid models using a real equation of state, when assuming full thermodynamic equilibrium between the phases. The Span-Wagner reference equation of state for CO_2 is used to describe phase equilibrium and thermodynamic properties.

The first approach consists in letting the flow evolve first without mass transfer, and then correct the solution to an equilibrium state using a fractional-step method. In this case the two-fluid model consists of two mass, two momentum and one energy equation. The second approach ensures thermodynamic phase equilibrium at all times, reducing the model from two to only one mass equation.

The five-equation model only involves equilibrium in pressure and temperature, thus its speed of sound is continuous in the transition to single phase. The full thermodynamic equilibrium assumption gives a discontinuous speed of sound in the transition between single and two-phase flow. The mixture speed of sound in the four-equation model is generally lower than the mixture speed of sound in the five-equation model.

The four-equation model introduced additional complexity in the calculation of the primitive variables from conserved quantities. The kinetic energy is constant during

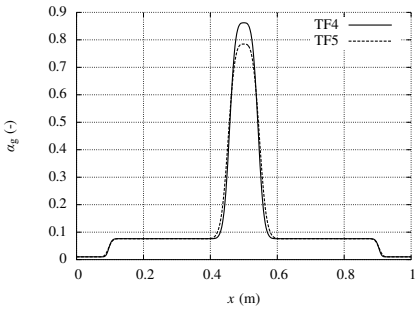

(a) Gas volume fraction.

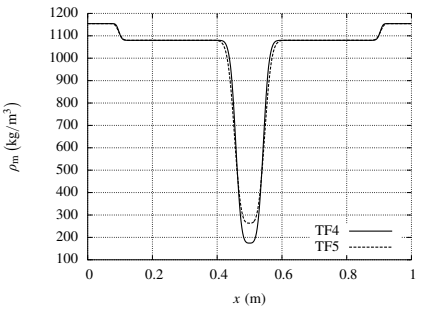

(b) Mixture density.

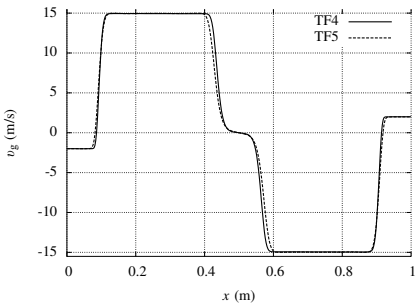

(c) Gas velocity.

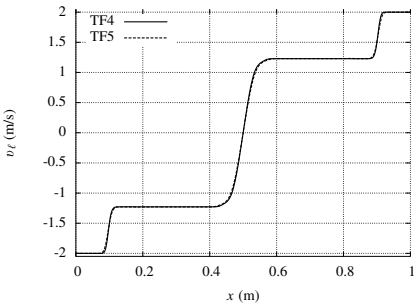

(d) Liquid velocity.

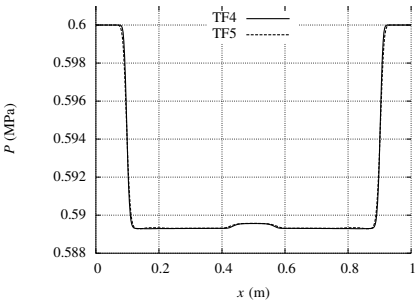

(e) Pressure.

Figure 12: Two-phase expansion tube simulated using the four-equation two-fluid model (TF4) and five-equation two-fluid model (TF5). Result at $t = 0.03$ s using CFL number 0.5 and 400 cells. The Riemann problem is solved using MUSCL–FORCE flux.

mass transfer with the fractional-step approach, but had to be determined by iteration in the four-equation model.

Second-order convergence is achieved for both models on a Gauss curve shaped volume-fraction wave advected in a constant flow field. The FORCE scheme and MUSCL with van Leer limiter together with a two-stage second-order strong-stability-preserving Runge–Kutta time integration was applied. The second-order MUSCL-FORCE scheme for both the four- and five-equation models also performed well on the discontinuous solutions of a shock tube.

Applying the four-equation model on a volume-fraction discontinuity propagating at constant velocity in an constant pressure field, no pressure or velocity oscillations were seen at the discontinuity.

A numerical test of a two-phase CO_2 expansion tube is performed applying both the four-equation and five-equation two-fluid model. The initial velocity discontinuity produces the same four expansion waves, the cavitation pocket, and the same qualitative behaviour is seen in the results as in the numerical example by Saurel et al. [22]. The numerical diffusion when solving the five-equation model is larger than when solving the four-equation model.

Mainly due to a larger time step in the four-equation model, the performance of the four-equation model was shown to be superior to that of the five-equation model. The performance was quantified as solution error per CPU time consumed.

To demonstrate the ability of the approach to handle transition from two-phase flow to single-phase flow, the four-equation model was applied to a separation case, where gravity separates an initially homogenous mixture of gas and liquid. By plotting the simulated pressure against temperature together with the CO_2 saturation line, gas-liquid transition to pure liquid was verified.

Acknowledgments

This work was supported by the CO_2 Dynamics project. The authors acknowledge the support from the Research Council of Norway (189978), Gassco AS, Statoil Petroleum AS and Vattenfall AB. We are grateful to our colleague Svend Tollak Munkejord, Tore Flåtten and Peder Aursand, for fruitful discussions.

References

[1] IEA, Energy Technology Perspectives, 2012. doi:10.1787/20792603.

[2] R. Saurel, R. Abgrall, A multiphase Godunov method for compressible multifluid and multiphase flow, J. Comput. Phys. 150 (2) (1999) 425–467.

[3] R. Saurel, O. Le Métayer, A multiphase model for compressible flows with interfaces, shocks, detonation waves and cavitation, J. Fluid Mech. 431 (2001) 239–271.

[4] H. Paillère, C. Corre, J. R. García Cascales, On the extension of the AUSM+ scheme to compressible two-fluid models, Comput. Fluids 32 (6) (2003) 891–916.

[5] O. Le Métayer, J. Massoni, R. Saurel, Elaborating equations of state of a liquid and its vapor for two-phase flow models, Int. J. Therm. Sci. 43 (3) (2004) 265–276.

[6] H. O. Nordhagen, S. Kragset, T. Berstad, A. Morin, C. Dørum, S. T. Munkejord, A new coupled fluid-structure modelling methodology for running ductile fracture, Comput. Struct. 94–95 (2012) 13–21. doi:10.1016/j.compstruc.2012.01.004.

[7] R. Span, W. Wagner, A new equation of state for carbon dioxide covering the fluid region from the triple-point temperature to 1100 K at pressures up to 800 MPa, J. Phys. Chem. Ref. Data 25 (6) (1996) 1509–1596. doi:10.1063/1.555991.

[8] P. J. Martínez Ferrer, T. Flåtten, S. T. Munkejord, On the effect of temperature and velocity relaxation in two-phase flow models, ESAIM – Math. Model. Num. 46 (2) (2012) 411–442. doi:10.1051/m2an/2011039.

[9] A. Morin, T. Flåtten, A two-fluid four-equation model with instantaneous thermodynamical equilibrium, Submitted for publication 2013. Preprint available from http://www.math.ntnu.no/conservation/2013/002.html.

[10] E. F. Toro, Riemann solvers and numerical methods for fluid dynamics, 2nd Edition, Springer-Verlag, Berlin, 1999.

[11] B. van Leer, Towards the ultimate conservative difference scheme V. A second-order sequel to Godunov's method, J. Comput. Phys. 32 (1) (1979) 101–136.

[12] M. Ishii, Thermo-fluid dynamic theory of two-phase flow, Collection de la Direction des Etudes et Recherches d'Electricité de France, Eyrolles, Paris, 1975.

[13] S. T. Munkejord, S. Evje, T. Flåtten, A MUSTA scheme for a nonconservative two-fluid model, SIAM J. Sci. Comput. 31 (4) (2009) 2587–2622. doi:10.1137/080719273.

[14] H. B. Stewart, B. Wendroff, Review article: Two-phase flow: Models and methods, J. Comput. Phys. 56 (3) (1984) 363–409.

[15] I. Toumi, A. Kumbaro, An approximate linearized Riemann solver for a two-fluid model, J. Comput. Phys. 124 (2) (1996) 286–300.

[16] D. Bestion, The physical closure laws in the CATHARE code, Nucl. Eng. Design 124 (3) (1990) 229–245.

[17] V. H. Ransom *et. al.*, RELAP5/MOD3 Code Manual, NUREG/CR-5535, Idaho National Engineering Laboratory, ID (1995).

[18] K. H. Bendiksen, D. Malnes, R. Moe, S. Nuland, The dynamic two-fluid model OLGA: Theory and application, SPE Production Engineering 6 (2) (1991) 171–180.

[19] J. H. Stuhmiller, The influence of interfacial pressure forces on the character of two-phase flow model equations, Int. J. Multiphase Flow 3 (6) (1977) 551–560.

[20] T. Flåtten, H. Lund, Relaxation two-phase flow models and the subcharacteristic condition, Math. Mod. Meth. Appl. S. 21 (12) (2011) 2379–2407. doi:10.1142/S0218202511005775.

[21] H. Lund, A hierarchy of relaxation models for two-phase flow, SIAM J. Appl. Math. 72 (6) (2012) 1713–1741. doi:10.1137/12086368X.

[22] R. Saurel, F. Petitpas, R. Abgrall, Modelling phase transition in metastable liquids: application to cavitating and flashing flows, J. Fluid Mech. 607 (2008) 313–350. doi:10.1017/S0022112008002061.

[23] H. Bruce Stewart, B. Wendroff, Two-phase flow: models and methods, J. Comput. Phys. 56 (3) (1984) 363–409.

[24] R. J. LeVeque, Finite Volume Methods for Hyperbolic Problems, Cambridge University Press, Cambridge, UK, 2002.

[25] F. Coquel, K. El Amine, E. Godlewski, B. Perthame, P. Rascle, A numerical method using upwind schemes for the resolution of two-phase flows, J. Comput. Phys. 136 (2) (1997) 272–288.

[26] M. L. Michelsen, State function based flash specifications, Fluid Phase Equilib. 158-160 (1999) 617 – 626. doi:10.1016/S0378-3812(99)00092-8.

[27] K. E. T. Giljarhus, S. T. Munkejord, G. Skaugen, Solution of the Span-Wagner equation of state using a density-energy state function for fluid-dynamic simulation of carbon dioxide, Ind. Eng. Chem. Res. 51 (2) (2012) 1006–1014. doi:10.1021/ie201748a.

[28] M. Hammer, Å. Ervik, S. T. Munkejord, Method using a density-energy state function with a reference equation of state for fluid-dynamics simulation of vapor-liquid-solid carbon dioxide, Ind. Eng. Chem. Res. 52 (29) (2013) 9965–9978. doi:10.1021/ie303516m.

[29] A. Morin, T. Flåtten, S. T. Munkejord, A Roe scheme for a compressible six-equation two-fluid model, Int. J. Numer. Meth. Fl. 72 (2013) 478–504.

[30] P. Aursand, T. Flåtten, On the dispersive wave-dynamics of 2×2 relaxation systems, J. Hyperbolic Differ. Equ. 9 (4) (2012) 641–659. doi:10.1142/S021989161250021X.

[31] S. Osher, Convergence of generalized MUSCL schemes, SIAM J. Numer. Anal. 22 (5) (1985) 947–961.

[32] D. I. Ketcheson, A. C. Robinson, On the practical importance of the SSP property for Runge-Kutta time integrators for some common Godunov-type schemes, Int. J. Numer. Meth. Fl. 48 (3) (2005) 271–303.

[33] R. Abgrall, S. Karni, Comment on the computation of non-conservative products, J. Comput. Phys. 229 (8) (2010) 2759–2763. doi:10.1016/j.jcp.2009.12.015.

[34] M. J. Castro, P. G. LeFloch, M. L. Muñoz-Ruiz, C. Parés, Why many theories of shock waves are necessary: Convergence error in formally path-consistent schemes, J. Comput. Phys. 227 (17) (2008) 8107–8129. doi:10.1016/j.jcp.2008.05.012.

[35] G. Dal Maso, P. G. LeFloch, F. Murat, Definition and weak stability of nonconservative products, J. Math. Pures Appl. 74 (6) (1995) 483–548.

[36] R. Abgrall, How to prevent pressure oscillations in multicomponent flow calculations: A quasi conservative approach, J. Comput. Phys. 125 (1) (1996) 150–160.

[37] R. Saurel, F. Petitpas, R. A. Berry, Simple and efficient relaxation methods for interfaces separating compressible fluids, cavitating flows and shocks in multiphase mixtures, J. Comput. Phys. 228 (5) (2009) 1678–1712, 10.1016/j.jcp.2008.11.002.